The competing effects of wall transpiration and stretching on Homann stagnation-point flow

P. D. Weidman
Department of Mechanical Engineering
University of Colorado
Boulder, CO 80309

Yi Ping Ma
Department of Applied Mathematics
University of Colorado
Boulder, CO 80309

Abstract

The simultaneous effects of normal transpiration through a radially stretching porous plate beneath Homann stagnation-point flow is considered. The exact similarity reduction of the Navier-Stokes equations depends on the stretching parameter λ and the transpiration parameter μ. Dual solutions are found over a limited range $\lambda_c < \lambda < -1$ in the case of suction ($\mu > 0$) but unique solutions exist for blowing ($\mu < 0$). It is shown that the range of dual solutions increases with μ, but a self-similar stability analysis reveals that the lower solution branches are unstable while upper solution branches are stable.

Keywords: Homann stagnation-point flow, transpiration, radial stretching, nonuniqueness, stability

1 Introduction

Many problems have addressed two-dimensional stagnation-point flow with a stretching boundary and/or a porous boundary with suction and/or blowing, sometimes for nanofluids and sometimes with an imposed magnetic field. Here we review relevant publications for axisymmetric Homann [1] stagnation-point flow for various plate boundary conditions. Wang [2] studied axisymmetric stagnation flow towards a moving plate. Weidman and Mahalingam [3] reported on the problem of Homann stagnation-point flow impinging on a transversely oscillating plate with suction. Attia [4] studied Homann hydromagnetic flow and heat transfer with uniform suction and injection. Velocity profiles were given for suction and injection in the absence of a magnetic field. Mahapatra and Gupta [5] reported on Homann stagnation-point flow impinging on a radially stretching surface. They find that a regular boundary-layer structure appears when the stretching velocity is less than the free stream velocity and that otherwise an inverted boundary

layer is formed. Wang [6] reported, *inter alia*, on Homann stagnation flow directed towards a shrinking sheet. Attia [7] studied Homann hydromagnetic point flow impinging on a radially stretching sheet with heat generation in which results were given in the absence of a magnetic field. No publications were found that included both radial stretching of, and transpiration through, the surface bounding Homann stagnation-point flow.

The focus of the present endeavor is twofold. First we consider the simultaneous effects of transpiration, characterized by parameter μ, and plate stretching, characterized by parameter λ, on the self-similar reduction of the Navier-Stokes equations. Second, the linear temporal stability of both the unique and dual solutions is determined.

The presentation proceeds as follows. In §2 the boundary-value problem for Homann [1] stagnation-point flow impinging on a porous stretching/shrinking plate with suction/blowing is formulated and solved numerically. An analysis of behavior near the right focal point is given in §2.1 and that near the left focal point is given in §2.2. The large μ and large λ asymptotic behaviors are given in §2.3 and §2.4, respectively. The stability of the unique and dual solutions encountered is determined following the method of Merkin [8] in §3. A discussion of results and concluding remarks are given in §4.

2 Formulation and solution

Consider axisymmetric Homann stagnation point flow for which (r, z) are the radial and axial coordinates with corresponding velocities (u, w). For flow above a flat porous disk, the unsteady continuity and Navier-Stokes equations for an incompressible fluid are

$$\frac{1}{r}\frac{\partial(ru)}{\partial r} + \frac{\partial w}{\partial z} = 0 \tag{1a}$$

$$\frac{\partial u}{\partial t} + u\,\frac{\partial u}{\partial r} + w\,\frac{\partial u}{\partial z} = -\frac{\partial p}{\partial r} + \nu\,\left(\frac{\partial^2 u}{\partial r^2} + \frac{1}{r}\frac{\partial u}{\partial r} + \frac{\partial^2 u}{\partial z^2} - \frac{u}{r^2}\right) \tag{1b}$$

$$\frac{\partial w}{\partial t} + u\,\frac{\partial w}{\partial r} + w\,\frac{\partial w}{\partial z} = -\frac{\partial p}{\partial z} + \nu\,\left(\frac{\partial^2 w}{\partial r^2} + \frac{1}{r}\frac{\partial w}{\partial r} + \frac{\partial^2 w}{\partial z^2}\right) \tag{1c}$$

wherein ρ is the fluid density and ν is the kinematic viscosity, both assumed constant, and p is the pressure. We adopt the unsteady similarity transformation

$$u(r,z) = ar f'(\eta), \qquad w(r,z) = -2\sqrt{a\nu}\,f(\eta), \qquad \eta = \sqrt{\frac{a}{\nu}}\,z, \qquad \tau = at \tag{2}$$

where a is the strain rate of the stagnation-point flow. Setting $f'(0) = \lambda$ gives linear radial stretching for $\lambda > 0$ and linear radial shrinking for $\lambda < 0$. Setting $f(0) = \mu$ gives uniform suction for $\mu > 0$ and uniform blowing for $\mu < 0$. The *ansatz* (2) satisfies the continuity equation (1a) and substitution into the unsteady Navier-Stokes equations (1b,c) gives

$$f''' + 2f\,f'' - f'^2 + 1 - f'_\tau = 0 \tag{3a}$$

$$f(0) = \mu, \qquad f'(0) = \lambda, \qquad f'(\infty) = 1. \tag{3b, c, d}$$

The compatible steady flow pressure field is

$$p(r, \eta) = p_0 - \rho \left[\frac{a^2 r^2}{2} + 2a\nu(f^2 + f') \right] \tag{4a}$$

where p_0 is the pressure at $r = \eta = 0$, namely

$$p_0 = 2\rho a \nu (\mu^2 + \lambda) \tag{4b}$$

Solutions of the steady flow problem for $f''(0)$, at each value of μ and λ, are related to the radial wall shear stress τ through the expression

$$\tau = \mu \frac{\partial u}{\partial z}\bigg|_{z=0} = \rho\, \nu^{1/2} a^{3/2}\, r\, f''(0) \tag{5}$$

showing that the shear stress increases linearly with radius.

We denote focal points in λ-$f''(0)$ space using $\{\lambda, f''(0)\}$. The obvious exact solution $f(\eta) = \eta$, valid for all transpirations μ, exists at the $\{1, 0\}$ focal point of the system. Solutions for $\mu = 0$ are those analyzed previously by Wang (2008). Numerical integrations carried out for μ = -0.5, -0.25, 0.0, 0.25 and 0.5 are displayed in λ-$f''(0)$ parameter space in Figure 1. Integrations carried out using a standard shooting method incurred difficulties at various negative values of λ. The integration method ODEINT found in Press, et al [9], has been used with great success on a number of problems, but in certain instances the shooting iteration becomes difficult as more and more precise values of $f''(0)$ are needed to obtain a converged solution. As a result, integrations were completed using the continuation code AUTO; see Doedel [10].

The results for suction ($\mu > 0$) in Figure 1 exhibit features similar to those found in the boundary-layer flows studied by Weidman, et al [11,12] and Bhattacharyya and Layek [13]: there is a region of unique solutions for $\lambda > -1$, dual solutions for $\lambda_c < \lambda \leq -1$ and no solutions for $\lambda < \lambda_c$. The critical values of λ_c accurate to four decimal places are provided in Table 1. For blowing ($\mu < 0$), on the other hand, solutions are unique for all $\lambda > -1$.

Sample similarity velocity profiles $f'(\eta)$ presented in Figure 2 quantify the effect of suction and blowing at positive λ. The results for $\lambda = 0.5$ corresponding to a disk stretching from the origin at half the speed of the free stream and those plotted for $\lambda = 1.5$ correspond to a disk stretching 50% faster than the free stream. In both cases suction increases the skin friction measured by $f''(0)$ and decreases the boundary layer thickness, while the opposite is true for blowing.

For negative values of λ the profiles along the curve $\mu = 0.5$ have unique solutions in the range $-1 \leq \lambda \leq 0$ and dual solutions in the range $-1.425 < \lambda \leq -1.0$. Velocity profiles along this curve are displayed in Figure 3a. For $\mu = -0.5$ there are only unique solutions for all $\lambda \geq -1$. Sample velocity profiles for $\mu = -0.5$ at selected values of λ are shown in Figure 3b.

Note that, in addition to the focal point at $\{1, 0\}$, there is another zero stress focal point at $\{-1, 0\}$. Analysis of solutions near these points helps to elucidate local solution behaviors. We consider each in turn in the following sections and also determine the asymptotic behavior of solutions for large μ and large λ.

2.1 Behavior near the focal point $\{1, 0\}$

Near the right focal point at $\lambda = 1$ we insert $\lambda = 1 - \epsilon$ and insert

$$f(\eta) = \eta + \mu - \epsilon\phi(\eta) \tag{6}$$

into the steady form of (3) and linearize for $\epsilon << 1$ to obtain the boundary-value problem

$$\phi''' + 2(\eta + \mu)\,\phi'' - 2\phi' = 0 \tag{7a}$$

$$\phi(0) = 0, \qquad \phi'(0) = 1, \qquad \phi'(\infty) = 0. \tag{7b, c, d}$$

The general solution for $\phi'(\eta)$ is readily found to be

$$\phi'(\eta) = C_1(\eta + \mu) + C_2\left[e^{-(\eta+\mu)^2} + \sqrt{\pi}(\eta + \mu)\mathrm{Erf}(\eta + \mu)\right] \tag{8a}$$

and application of boundary conditions (7c,d) gives the constants

$$C_1(\mu) = \frac{-\sqrt{\pi}}{e^{-\mu^2} + \mu\sqrt{\pi}(\mathrm{Erf}(\mu) - 1)} \tag{8b}$$

$$C_2(\mu) = \frac{1}{e^{-\mu^2} + \mu\sqrt{\pi}(\mathrm{Erf}(\mu) - 1)} \tag{8c}$$

wherein $\mathrm{Erf}(z)$ is the error function; see Abramowitz and Stegun [14]. We use these results to compute the slope of the parametric solution curves at the focal point, *viz.*

$$\left.\frac{d\,f''(0)}{d\lambda}\right|_{\lambda=1} = C_1(\mu) + C_2(\mu)\sqrt{\pi}\,\mathrm{Erf}(\mu). \tag{9}$$

Focal point slopes computed numerically at $\mu = \{-0.5, -0.25, 0.0, 0.25, 0.50\}$ exhibit excellent agreement with the analytical result (9) in Figure 4.

2.2 Behavior near the focal point $\{-1, 0\}$

The analysis near the left focal point at $\lambda = -1$ is more difficult. All we can do in this case is evaluate the the steady governing equation (3a) at $\eta = 0$ using boundary conditions (3b,c) to obtain

$$f'''(0) + 2\mu f''(0) - \lambda^2 + 1 = 0. \tag{10}$$

Differentiation with respect to λ gives

$$\frac{df'''(0)}{d\lambda} + 2\mu\frac{df''(0)}{d\lambda} - 2\lambda = 0. \tag{11}$$

Evaluation at $\lambda = -1$ gives

$$\frac{df'''(0)}{d\lambda} + 2\mu\frac{df''(0)}{d\lambda} = -2 \tag{12}$$

and numerical calculations suggest that the first term is zero which furnishes the result

$$\left.\frac{d\,f''(0)}{d\lambda}\right|_{\lambda=-1} = -\frac{1}{\mu}. \tag{13}$$

We compare the slopes given by (13) at $\mu = -0.5$ and $\mu = 0.5$ with the numerical results in Figure 1.

2.3 Large μ asymptotics

Of practical interest is the asymptotic behavior of solutions for large suction. When $\mu \gg 1$, the flow is fully viscous in the vicinity of the plate. Introducing

$$\xi = \mu\eta, \qquad f(\eta) = \mu + \frac{h(\xi)}{\mu} \tag{14}$$

into the steady form of (3) yields the boundary-value problem

$$h''' + 2h'' = 0; \qquad h(0) = 0, \quad h'(0) = \lambda, \quad h'(\infty) = 1 \tag{15}$$

where now a prime denotes differentiation with respect to ξ. The solution, rewritten in terms of the original similarity variable η, is given by

$$f(\eta) = \mu + \eta + \frac{\lambda - 1}{2\mu}\left(1 - e^{-2\mu\eta}\right). \tag{16}$$

The large μ approximation for the shear stress parameter is then

$$f''(0) = 2\mu\,(1 - \lambda) \qquad\qquad (\mu \gg 1). \tag{17}$$

A comparison of this asymptotic behavior with the numerically determined values of $f''(0)$ for $\lambda = \{0.0, 0.5, 1.0, 1.5, 2.0\}$ shown in Figure 5 reveals that the asymptotic formula (17) provides accurate values of the shear stress parameter for all λ when $\mu \geq 8.0$.

2.4 Large λ asymptotics

Inspection of boundary-value problem (3), with $\lambda \gg 1$, suggests the rescaling

$$\eta = \lambda^{-\alpha}\xi, \qquad f(\eta) = \lambda^{\alpha} F(\xi) \tag{18}$$

which maintains the form of the differential equation in (3) and yields

$$F''' + 2FF'' - F'^2 + \lambda^{-4\alpha} = 0 \tag{19a}$$

$$F(0) = \lambda^{-\alpha}\mu, \qquad F'(0) = \lambda^{1-2\alpha}, \qquad F''(\infty) = \lambda^{-3\alpha} \tag{19b, c, d}$$

where a prime now denotes differentiation with respect to ξ. On setting $\alpha = 1/2$ to obtain $F'(0) = 1$, a suitable solution *ansatz* is

$$F(\xi) = F_0(\xi) + \mu\lambda^{-1/2}F_1(\xi) + \lambda^{-1}F_2(\xi) + \ldots \tag{20}$$

in which, according to (19), the first two functions are governed by the boundary-value problems

$$F_0''' + 2F_0F_0'' - F_0'^2 = 0$$

$$F_0(0) = 0, \qquad F_0'(0) = 1, \qquad F_0''(\infty) = 0$$

and

$$F_1''' + 2(F_0F_1'' - F_0'F_1' + F_0''F_1) = 0$$

$$F_1(0) = 1, \qquad F_1'(0) = 0, \qquad F_1''(\infty) = 0.$$

The factor μ in (20) was anticipated by noting that the problem for F_1 is linear and forced solely by its initial value. Then the asymptotic form of a level μ curve in the $\lambda - f''(0)$ plane is given, according to (18) and (20), by

$$f''(0) = \lambda^{3/2} F''(0) \sim \lambda^{3/2} F_0''(0) + \lambda\mu F_1''(0) \qquad (\lambda \gg 1). \tag{21}$$

Numerical integrations give $F_0''(0) = -1.17372$ and $F_1''(0) = -1.06643$. A comparison of the two-term asymptotic results with the numerically computed values of $f''(0)$ at $\mu = \{-1.0, -0.5, 0.0, 0.5, 1.0\}$ is given in Figure 6.

3 Flow Stability

We compute the self-similar linear temporal stability of the flow following Merkin [8]. Thus, to test stability of the steady flow solution $f(\eta) \equiv F_0(\eta)$ satisfying the steady boundary-value problem (3), we write for the unsteady problem

$$f(\eta, \tau) = F_0(\eta) + e^{-\alpha\tau} G(\eta) \tag{22}$$

where $G(\eta)$ is small relative to $F_0(\eta)$. Inserting this time-dependent solution form into (3) furnishes the linearised problem

$$G''' + 2(F_0 G'' + F_0'' G) - 2F_0' G' + \gamma G' = 0 \tag{23a}$$

$$G(0) = 0, \qquad G'(0) = 0, \qquad G'(\infty) = 0. \tag{23b, c, d}$$

Solutions of (23) with its homogeneous boundary conditions are obtained by setting $G''(0) = 1$ and varying γ. Results for $\mu = \{-0.5, -0.25, 0.0, 0.25, 0.5\}$ are plotted in Figure 7. Each turning point crossing $\gamma = 0$ for $\mu \geq 0$ coincides with the turning points in Figure 1 as listed in Table 1. The results show that the lower branch solutions for $\mu = 0.25$ and 0.5 are unstable while the upper branch solutions are stable. The unique solutions for $\mu = 0, -0.25$ and -0.5 are everywhere stable.

4 Summary and conclusion

The problem of Homann [1] stagnation-point flow over a permeable flat plate is solved to exhibit the combined effects of wall transpiration and plate stretching. The existence and multiplicity of solutions are clearly displayed in the $\lambda - f''(0)$-parameter space for sample values of the suction parameter μ. In particular, for suction($\mu > 0$) dual solutions exist for $\lambda_c < \lambda \leq -1$ and no solutions eixst for $\lambda < \lambda_c$. For blowing ($\mu < 0$), on the other hand, solutions are unique for all $\lambda > -1$. The solutions presented here represent an exact similarity reduction of the Navier-Stokes equations.

Stability of the solutions is determined by adapting the linear temporal stability analysis of Merkin [8]. We find that the lower branches for $\mu > 0$ are unstable and the upper branches are stable. Also the solution branches for $\mu \leq 0$ are everywhere stable.

A possible study for future consideration would be to compute the effects of transpiration and radial stretching on the axisymmetric rotational stagnation-point flow reported by Agrawal [15].

References

1. Homann, F.: Der Einfluss grosser Zähigkeit bei der Strömung um den Zylinder und um die Kugel, Z. angew. Math. Mech., **16**, 153-164 (1936).

2. Wang, C. Y.: Axisymmetric stagnation flow towards a moving plate, AiChE J., **19**, 1080-1081 (1973).

3. Weidman, P. D. and Mahalingham, S.: Axisymmetric stagnation-point flow impinging on a transversely oscillating plate with uniform suction, J. Engng. Math., **31**, 305-318 (1997).

4. Attia, H. A: Homann magnetic flow and heat transfer with uniform suction or injection, Can. J. Phys., **81**, 1223-1230 (2003).

5. Mahapatra, T. R. and Gupta, A. S.: Stagnation-point flow towards a stretching sheet, Can. J. Chem. Engr., **81**, 258-263 (2003).

6. Wang, C. Y.: Stagnation flow towards a shrinking sheet, Int. J. Non-Linear Mech., **43**, 377-382 (2008).

7. Attia, H. A.: Steady three-dimensional hydromagnetic stagnation point flow towards a stretching sheet with heat conduction, Italian J. Pure Appl. Math., **27**, 9-18 (2010).

8. Merkin, J. H.: On dual solutions occurring in mixed convection in a porous medium, J. Engng. Math., **20**, 171-179 (1985).

9. W. H. Press, B. P. Flannery, S. A. Teukolsky and W. T. Vetterling, *Numerical Recipies*, Cambridge University Press, Cambridge (1989).

10. Doedel, E. J. AUTO-07p: Continuation and bifurcation software for ordineary differential equations (with HOMCONT). http://indy.cs.concordia.ca/auto/ (2012).

11. Weidman, P. D., Kubitschek, D. G., and Davis, A. M. J.: The effect of transpiration on self-similar boundary-layer flow over moving surfaces. Int. J. Engr. Sci., **44**, 730-737 (2006).

12. Weidman, P. D., Davis, A. M. J. and Kubitschek, D. G.: Crocco variable formulation for uniform shear flow over a stretching surface with transpiration: Multiple solutions and stability. Zeit. angew. Math. Phys., **58**, 313-332 (2008).

13. Bhattacharyya, K. and Layet, G. C.: Effects of suction/blowing on steady boundary layer stagnation-point flow and heat transfer towards a shrinking sheet with thermal radiation. Int. J. Heat Mass Trans., **54**, 302-307 (2011).

14. Abramowitz, M. and Stegun, I.: Handbook of Mathematical Functions, US Government Printing Office, Washington (1972).

15. Agrawal, H. L. A new exact solution of the equations of viscous motion with axial symmetry, Quart. J. Mech. Appl. Math., **10**, 42-44 (1957).

μ	λ_c
0.50	-1.425
0.25	-1.175
0.00	-1.0

Table 1. Variation of λ_c with transpiration parameter μ.

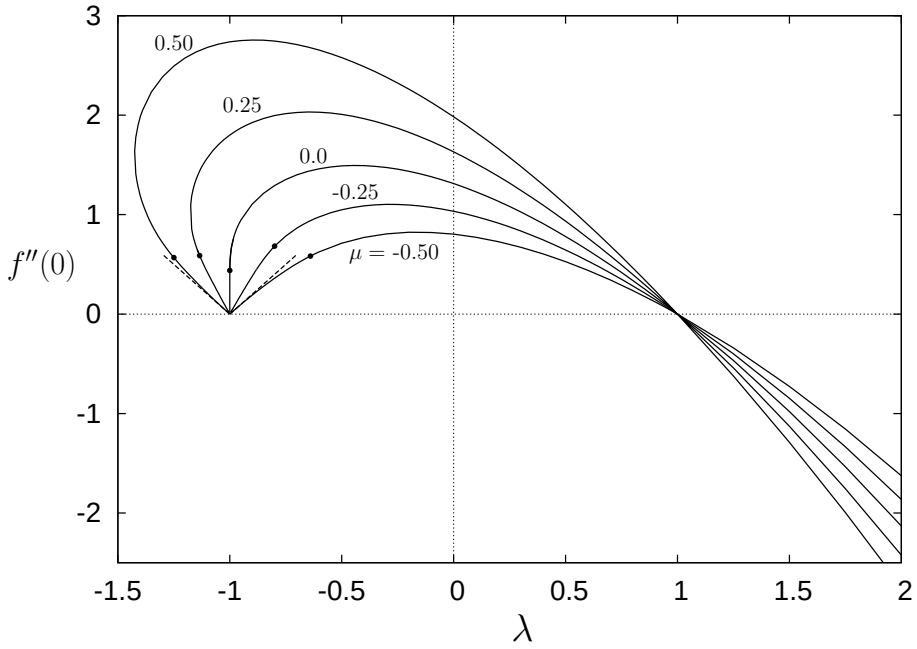

Figure 1. Parametric solution curves of $f''(0)$ as a function of λ for selected values of μ indicated. The dots show the demarcation between curves computed using a FORTRAN shooting code and the final approach to the focal point at $\lambda = -1$ using AUTO. The dashed lines are the slope of the curves given by Eq. (13) at the left focal point for $\mu = -0.5$ and 0.5.

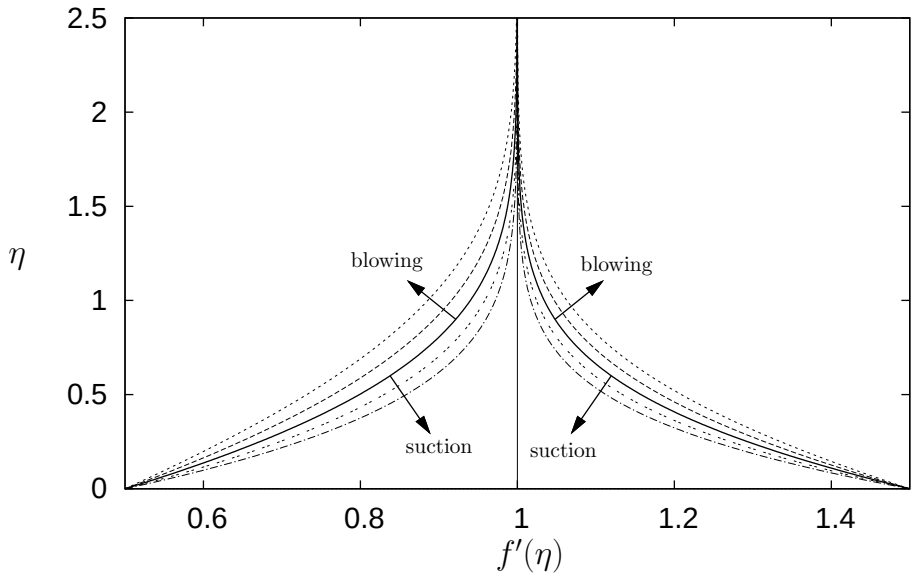

Figure 2. Velocity profiles for $\lambda = 0.5$ and $\lambda = 1.5$ showing the effects of suction and blowing about the zero transpiration profile marked as a solid line. The values of μ are {-0.50, -0.25, 0.0, 0.25, 0.50}.

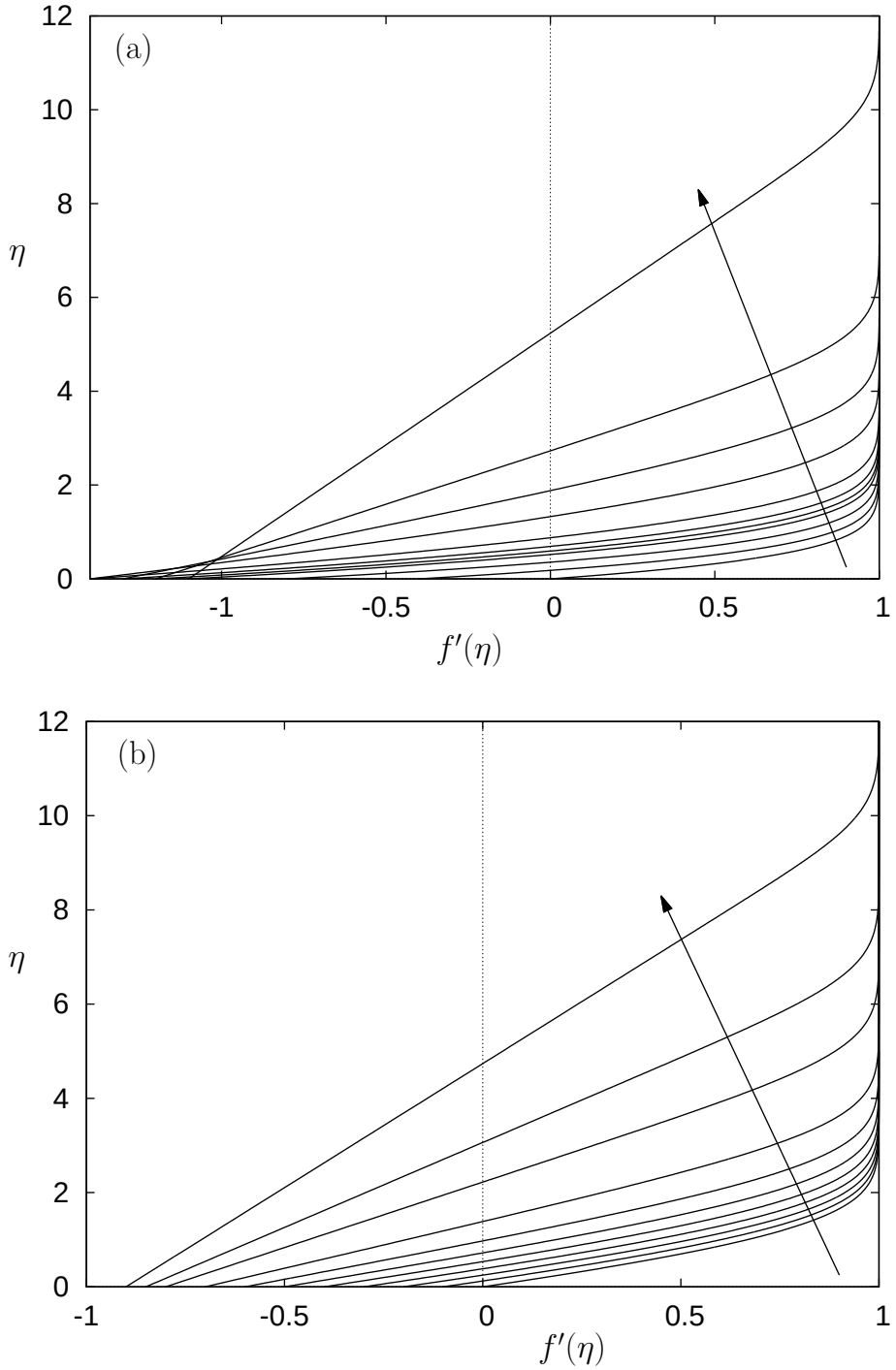

Figure 3. Velocity profiles: (a) along $\mu = 0.5$ at the successive values of $\lambda = \{0.0, -0.4, -0.8, -1.1, -1.2, -1.3, -1.4, -1.4, -1.3, -1.2 - 1.1\}$ as indicated by the arrow, and (b) along the curve $\mu = -0.5$ at the successive values of $\lambda = \{0.0, -0.1, -0.2, -0.3, -0.4, -0.5, -0.6, -0.7, -0.8, -0.85, -0.9\}$ as indicated by the arrow.

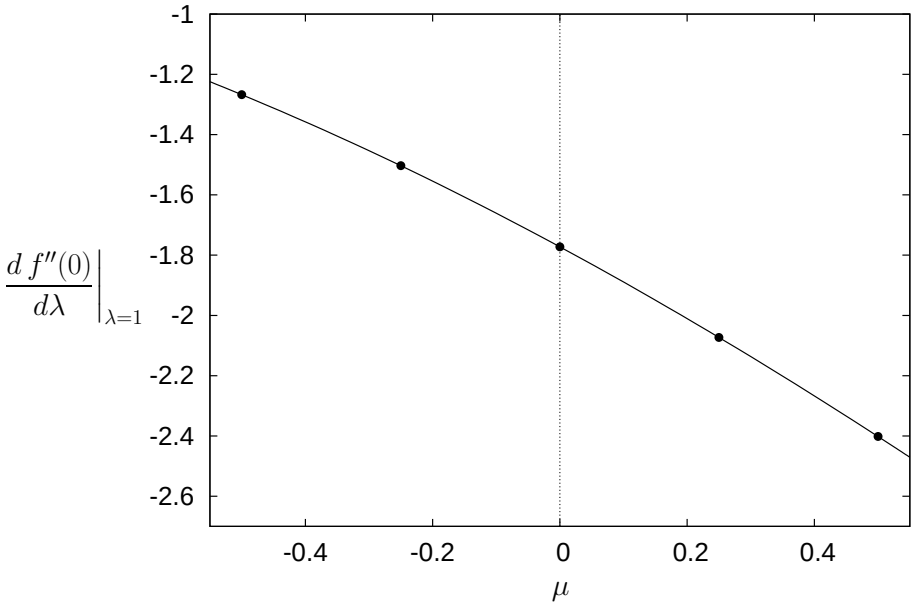

Figure 4. A comparison of numerically computed (solid circles) slopes of $f''(0)$ as a function of λ at the right focal point $\{1,\, 0\}$ with the theoretical prediction (line) given by Eq. (9).

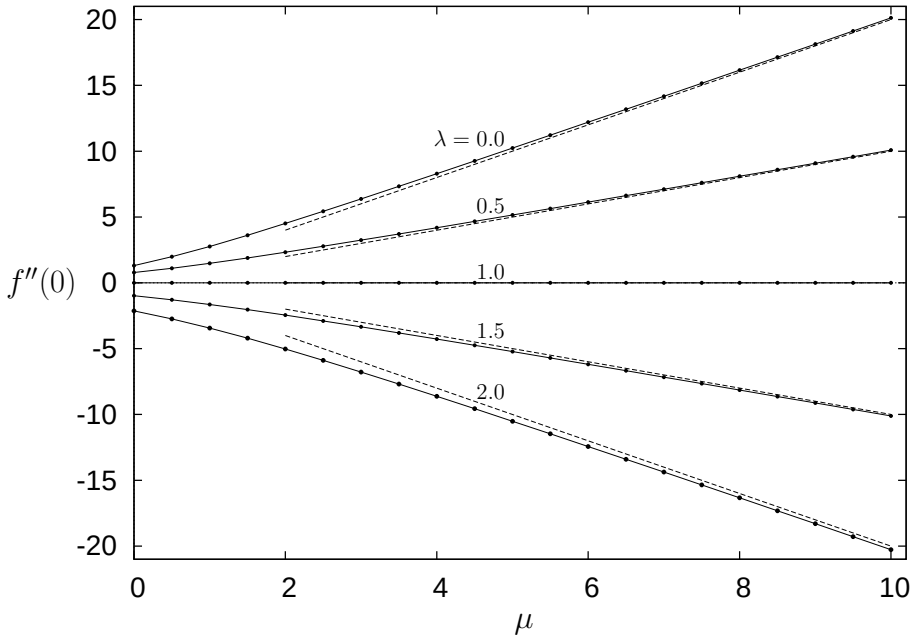

Figure 5. Comparison of numerically computed values of $f''(0)$ (solid dots) with their large μ asymptotic values given by Eq. (17) (dashed lines) as a function of μ at selected values of λ.

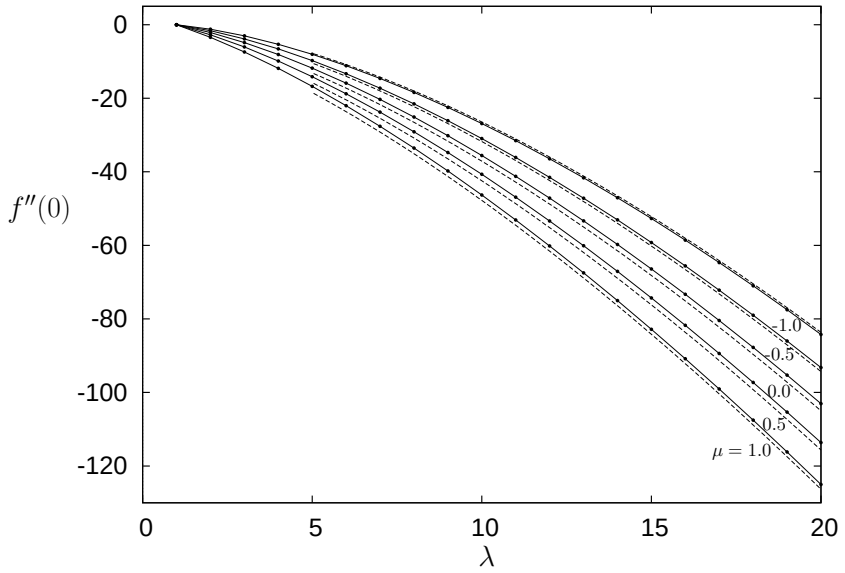

Figure 6. Comparison of numerically computed values of $f''(0)$ (solid dots) with their large λ asymptotic behaviors given by Eq. (21) (dashed lines) as a function of λ for selected values of μ.

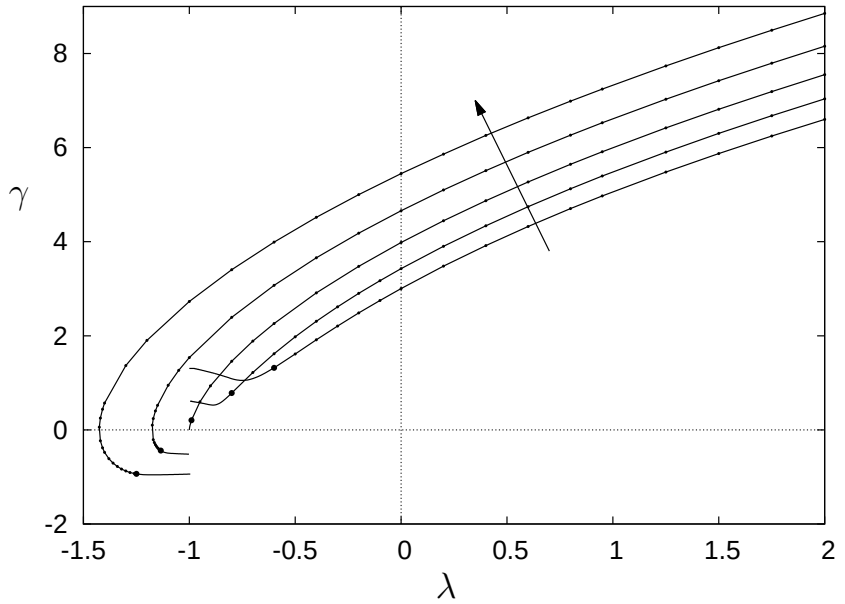

Figure 7. Smallest eigenvalues γ determined from the numerical solution of Eq. (23) for $\mu = \{-0.5, -0.25, 0.0, 0.25, 0.5\}$ as a function of λ in which the arrow shows the direction of increasing μ. The turning points for $\mu = 0.25$ and 0.5 are equal to the turning points for the parametric curves shown in Figure 1. The five large dots show the demarcation between curves computed using a FORTRAN shooting code (small dots) and the final approach to $\lambda = -1$ using AUTO (continuous lines).